Global Journal of Engineering and Technology Advances
eISSN: 2582-5003
Cross Ref DOI: 10.30574/gjeta
Journal homepage: https://gjeta.com/

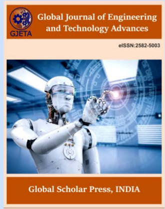

(Research Article)

Check for updates

FINITE ELEMENT MODELING OF REINFORCED CONCRETE DEEP BEAMS TO STUDY SIZE AND SHEAR REINFORCEMENT EFFECT

Ebtihaj Abu Elgasim Mohamed Ahmed *, Mohammed Motasim Hamoda Mohammed, Taha Mohammed Jaafar Abd Alrahman and Alyaa Omer Mustafa Mohammed

Structure department /School of Civil Engineering /Sudan University of Science and Technology.
* Corresponding Author

ORCID Details
Ebtihaj Abu Elgasim Mohamed Ahmed: https://orcid.org/0009-0005-0452-0016

Global Journal of Engineering and Technology Advances, 2026, 28(02), 163–186

Publication history: Received on 13 July 2026; revised on 19 August 2026; accepted on 21 August 2026

Article DOI: https://doi.org/10.30574/gjeta.2026.28.2.0222

ABSTRACT

Reinforced concrete deep beams are structural members characterized by relatively small span-to-depth ratios and nonlinear stress distributions. Because of their high shear capacity and ability to transfer concentrated loads, they are commonly used in transferring girders, pile caps, offshore structures, and other critical structural applications. Their behavior differs from that of slender beams because shear deformation, disturbed regions, diagonal cracking, and compression strut action strongly influence their load-transfer mechanism.

This study investigates the effects of beam size, web reinforcement, and beam width on the nonlinear behavior of reinforced concrete deep beams. Three groups of specimens were considered, with variations in overall depth, section width, and reinforcement arrangement. The investigation focused on load–deflection response, crack initiation, plastic strain distribution, shear capacity, and internal compressive force paths.

A three-dimensional nonlinear finite element model was developed using ABAQUS, and the Concrete Damaged Plasticity model was adopted to simulate concrete cracking, crushing, stiffness degradation, and inelastic response. The numerical results were validated against experimental data in terms of load–deflection behavior, crack development, and failure response. The comparison showed a good agreement between the finite element predictions and the experimental results, demonstrating the reliability of the calibrated numerical model.

The results indicate that increasing beam depth and width improve stiffness, increase load-carrying capacity, reduce midspan deflection, and delays crack formation. Beams with increased width and without stirrups developed lower plastic strain and greater crack resistance than narrower beams with web reinforcement. These findings confirm the significant role of beam geometry in controlling the structural response of reinforced concrete deep beams and demonstrate the effectiveness of nonlinear finite element analysis as a tool for investigating their behavior.

Keywords: Reinforced Concrete Deep Beams; Nonlinear Finite Element Analysis; ABAQUS; Concrete Damaged Plasticity; Size Effect; Web Reinforcement; Beam Width; Plastic Strain.

1 INTRODUCTION

Reinforced concrete is one of the most fundamental structural materials in civil engineering, owing to its ability to combine the high compressive strength and durability of concrete with the tensile resistance and ductility provided by embedded steel reinforcement [1]. Among various reinforced concrete elements, deep beams represent a critical class of structural members characterized by small span-to-depth ratios, substantial disturbed stress regions (D-regions), highly non-planar strain distributions, and shear-dominated failure modes [2], [3]. Unlike conventional slender beams, where simple Bernoulli-Euler flexural theory applies, the load-transfer mechanism in deep beams is complex and governed by shear deformation, diagonal tension cracking, direct arch action, and compression strut mechanisms [2], [4].

International structural design codes classify deep beams based on specific span-to-depth geometric limits. The British Standard BS 8110 [5] classifies a beam as deep when the span-to-depth ratio is 2.0 or less. Meanwhile, the Comité Euro-International du Béton (CEB) [6] sets limiting ratios of less than 2.0 for simply supported beams and 2.5 for continuous members. Conversely, Appendix A of the American Concrete Institute code (ACI 318) [7] adopts a broader definition, permitting classification as a deep beam for clear span-to-overall-depth ratios up to 4.0 [2]. Because linear elastic flexural assumptions fail in these elements due to non-linear force flow, the strut-and-tie model (STM) is widely employed to idealize internal force transfers into concrete compression struts, steel tension ties, and highly stressed nodal zones [8]. Furthermore, extensive research demonstrates that member depth, beam width, shear span-to-depth ratio (a/d a/d and web reinforcement arrangements heavily dictate ultimate shear strength, failure modes, and size effect phenomena [9], [10].

Nonlinear finite element analysis (NLFEA) offers a comprehensive and cost-effective approach for exploring the structural response of deep beams, particularly when large-scale physical testing is constrained. In particular, the Concrete Damaged Plasticity (CDP) constitutive model in ABAQUS has gained wide acceptance for simulating complex concrete behaviors, including tensile cracking, compressive crushing, stiffness degradation, and post-yield plastic strain development [11], [12]. Recent numerical studies underscore that accurate calibration of CDP material parameters, tensile fracture energy, and damage evolution rules is vital for predicting non-linear load–deflection response, cracking loads, and ultimate capacity [13]– [15]. Moreover, advanced continuum modeling has been successfully extended to simulate deep beams incorporating fiber-reinforced polymer (FRP) bars, recycled aggregate concretes, and steel fibers [16], [17]. Building upon these findings, the present study utilizes validated 3D ABAQUS finite element models to systematically examine the interactive effects of beam size, transverse web reinforcement, and cross-sectional width expansion on load–deflection response, plastic strain patterns, crack distribution, and force-transfer mechanisms.

2 METHODOLOGY

The nonlinear numerical investigation was carried out using the ABAQUS finite element software package. The modeling framework was developed to simulate the inelastic response of reinforced concrete deep beams under applied loading. This section presents the adopted concrete material model, with particular emphasis on the CDP approach, as well as the principal structural assumptions, element idealizations, boundary conditions, and kinematic considerations incorporated into the finite element models.

2.1 Concrete damaged plasticity model

The CDP model was adopted to represent the nonlinear mechanical behavior of concrete under both compressive and tensile loading conditions. This model is suitable for simulating the progressive degradation of stiffness associated with cracking in tension and crushing in compression. In the present study, CDP was used to capture the inelastic response, damage evolution, and failure mechanisms of reinforced concrete deep beams subjected to monotonic loading.

The CDP formulation combines isotropic damaged elasticity with tensile and compressive plasticity, allowing concrete stiffness reduction to be defined separately in tension and compression. The main material parameters include the dilation angle, eccentricity, the ratio of biaxial to uniaxial compressive strength, the shape factor of the yield surface, and the viscosity parameter. These parameters influence convergence behavior, post-cracking response, and the overall numerical stability of the finite element model.

By incorporating tensile cracking, compressive crushing, and stiffness degradation, the CDP model provides a reliable framework for predicting the load–deflection response, crack development, plastic strain distribution, and failure mode of reinforced concrete deep beams. Therefore, it was selected as the principal constitutive model for the nonlinear finite element analysis conducted in this study.

Table 1: Difference Between Deep Beams and Ordinary Beams [3]

Difference	**Deep beams**	**Ordinary beams**
Plan section	Plan section before bending does not remain plan after bending.	Plan section before bending remains plan after bending.
Strains	Resultant strains are not linear.	Resultant strains are linear.
Shear deformation	Shear deformation becomes significant compared to pure flexure.	Shear deformation is neglected.
Stress block	Stress blocks are not linear.	Stress block considered linear.
State of stresses	It is subjected to two-dimensional state of stress	Subjected to one-dimensional state of stresses.

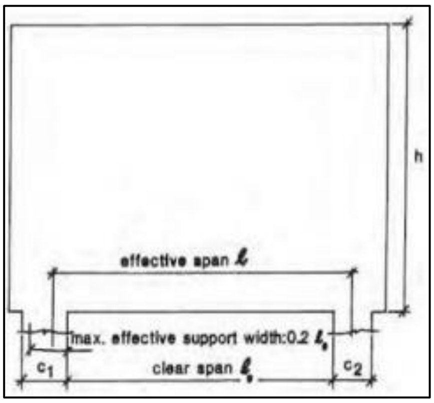

Figure 1: Single span [8]

Figure 2: Single span [14]

2.2 Compressive Force Path Concept

The Compressive Force Path (CFP) concept posits that the load-carrying capacity of a reinforced concrete member depends directly on the concrete strength along the compressive stress trajectory to the supports (Figure 3). Failure is triggered by transverse tensile stresses developing along this path due to three primary mechanisms:

- Path Direction Changes: Deviations in the stress path generate transverse tensile equilibrium forces (T in Figure 3).

- Stress Field Variation: Peak stresses at the narrowest path sections cause severe material dilation, inducing transverse tension (t_1 in Figure 3) in adjacent concrete.
- Inclined Crack Tips: High tensile stresses (t_2 in Figure 3) act perpendicular to the maximum principal compressive stress near crack tips [10].

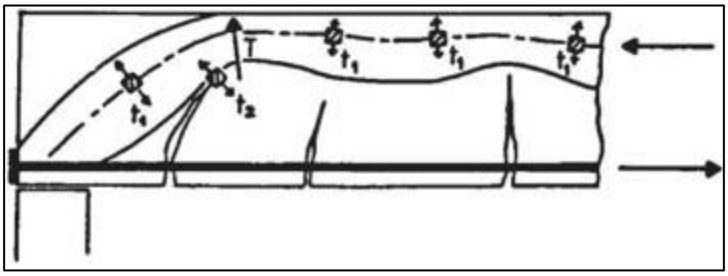

Figure 3: Compressive Force Path [10]

2.3 Deep Beam Design:

The strut-and-tie method (S.T.M) for the design of D-regions an emerging methodology for the design of all types of D-Regions is to envision and design an internal truss, consisting of concrete compressive struts and steel tension ties that are interconnected at nodes, to support the imposed loading through the boundaries of the discontinuity region. This design methodology is called the STM. The design process involves the steps described below. These steps are illustrated using a variety of D-Region design examples including a corbel, a corner joint, a dapped-ended beam, and a deep beam.

Define the boundaries of the D-Region and determine the imposed local and sectional forces.

Sketch the internal supporting truss, determine equivalent loadings, and solve for truss member forces.

Select reinforcing or prestressing steel to provide the necessary tie capacity and ensure that this reinforcement is properly anchored in the nodal zone (joint of the truss).

Evaluate the dimensions of the struts and nodes, such that the capacity of these components (struts and nodes) is sufficient to carry the design forces values. Provide distributed reinforcement to ensure ductile behavior of the D-Region. All the moments, shear and axial forces and reactions acting on the D- region must be known before modeling of D-regions can commence.[1]

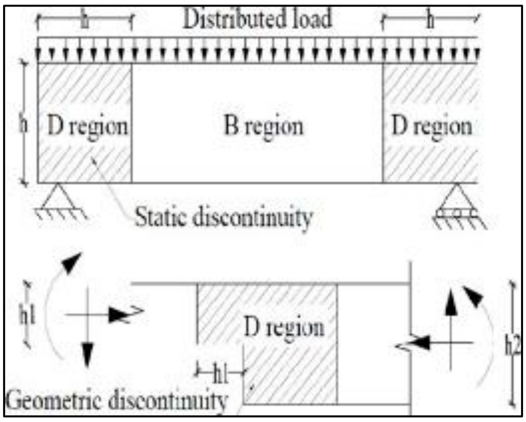

Figure 4: D and B region [3]

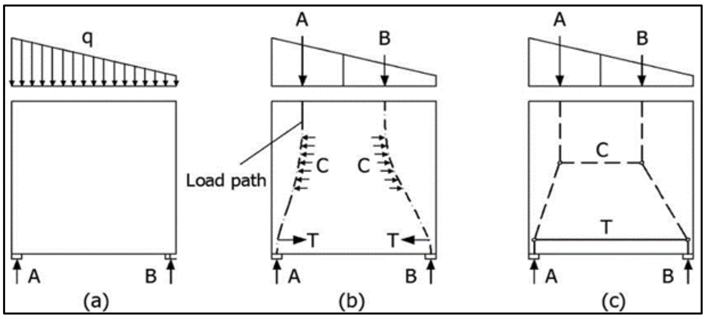

Figure 5: The load path meth [12]

Usually, the load path method can be used to systematically develop strut-and-tie models by tracing flow of forces through the structure. The S.T.M is based on the lower-bound theory of plasticity. Therefore, the actual capacity of the structure is equal to or greater than that of the idealized truss [3].

2.3.1 Design Procedures of the Strut-and-Tie Model:

The following procedure is adopted to develop the strut-and-tie model for the deep beam:

- First, the strut-and-tie model is drawn to scale. The expected load path is then established by examining the flow of internal forces, with support from finite element analysis where appropriate.
- The internal force system is then idealized as a strut-and-tie model. In this idealization, concrete compression fields are represented by struts; tensile force paths are represented by ties, and the regions where these members intersect are represented by nodal zones.
- After the model is established, its geometry is defined by locating the nodes at the intersections of the struts, ties, applied loads, and reactions. Once the geometry is known, the forces in each strut and tie are calculated using equilibrium conditions and basic principles of statics. These internal forces represent the load-resisting mechanism of the member.
- Finally, the dimensions of the concrete compression struts, the size of the nodal zones, and the required reinforcement details are determined based on equilibrium and ultimate strength requirements. The effective cross-sectional area of each strut is governed by the dimensions of the nodal zones at its ends. These nodal zones must be sufficiently large to keep stresses within the allowable limits specified by the design code, while remaining compatible with the geometric constraints of the D-region.[12]

2.4 Beam Information's

Three groups of reinforced concrete deep beams were considered, with each group consisting of three specimens. The overall beam height, h, varied proportionally from 500 mm to 1000 mm, while the widths of the loading and support plates, w_e, ranged from 75 mm to 150 mm. All specimens were tested to failure under two-point loading, with the applied loads positioned to avoid eccentricity. The beams were designed with a constant shear span-to-effective depth ratio, a/d, of 1.1 and a similar longitudinal reinforcement ratio, ρ_s, of approximately 1.2%. The details of the specimens are shown in figure (6)-(7).

In the specimen designation system, the lowercase letter **"b"** indicates specimens with proportionally increased beam width, whereas **"w"** denotes the presence of web reinforcement [11].

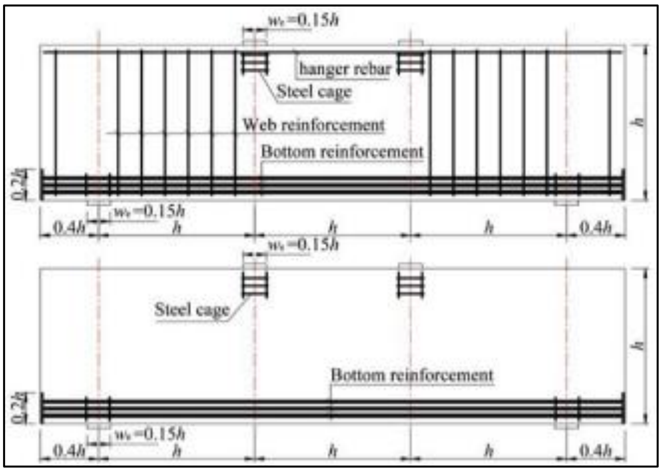

Figure 6: Typical reinforcement layout for specimens with and without web rebars [11]

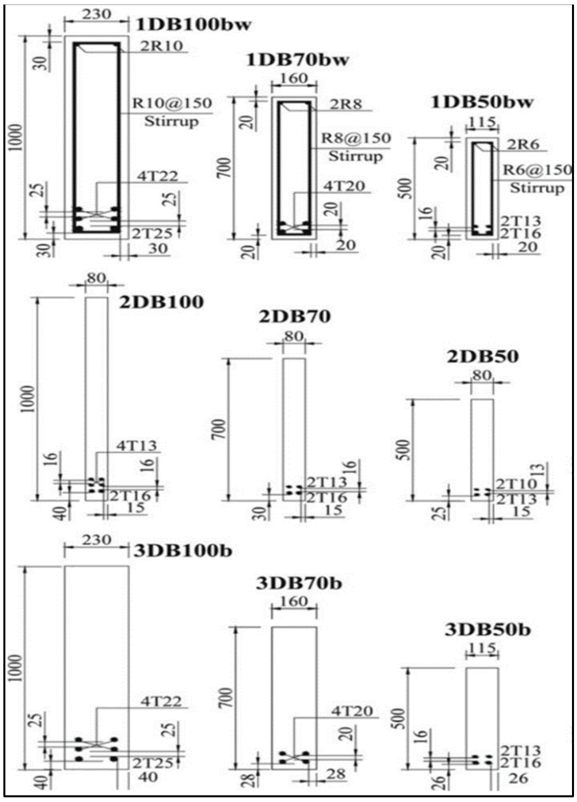

Figure 7: Beam cross-sections of 3 groups of beams [11]

Table 2: Summary of steel bar properties [11]

Type of Rebars	Nominal Yield Strength f_y (MPa)	Nominal Ultimate Strength f_u (MPa)	Young's Modulus E_s (GPa)
R6	426	488	195
R8	370	372	199
R10	455	522	190
T10	469	622	198

T13	520	611	190
T16	499	648	194
T20	522	592	193
T22	555	614	197
T25	520	639	193

2.4.1 Experimental work and test setup

Typical experimental test arrangements for the small, medium, and large beam specimens are presented in Figure (8) [11]. All specimens were tested simply supported by members under two-point loading. For the large beams with an overall height of 1000 mm, the two concentrated loads were applied using two 100-ton actuators. For the medium beams with heights of 500 mm and 700 mm, a steel spreader beam was used to distribute the actuator load into two equal point loads. In the case of small beams with a height of 350 mm, the swivel head of the actuator functioned as the spreader beam. The computer-controlled actuator could operate in either load-control or displacement-control mode. The spreader beam was supported on one pin and one roller placed on the upper surface of the specimen. The loading positions were carefully calibrated using a mini-laser projector to minimize load eccentricity in both the in-plane and out-of-plane directions of the beams.

2.4.2 Load control

(a)

(b)

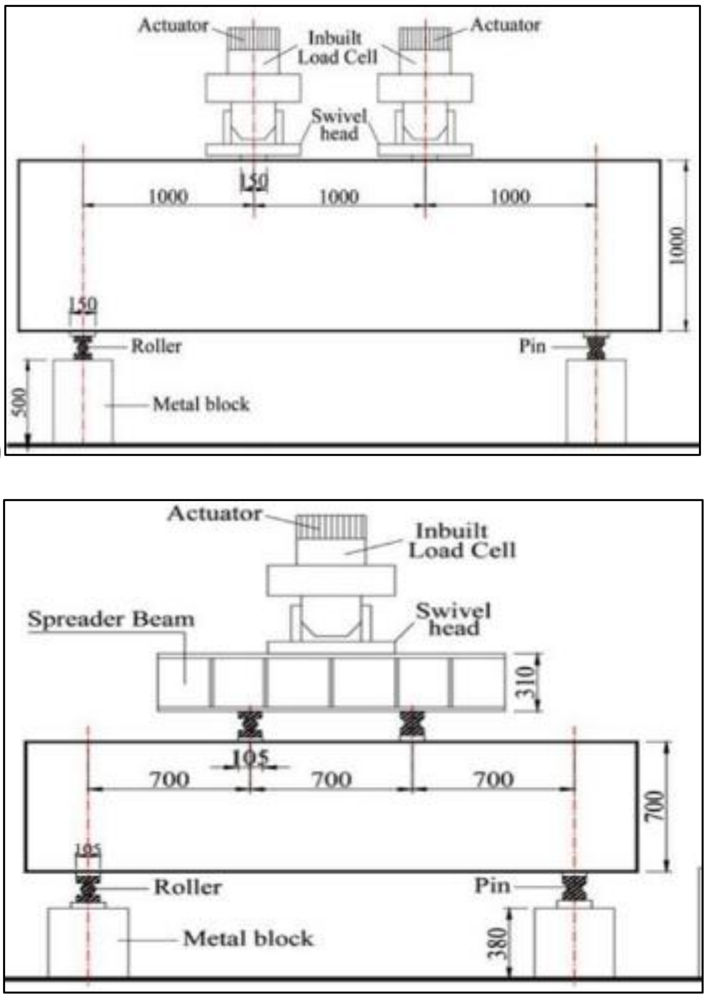

Figure 8: a, b Typical test setup for large and medium beams [11]

The specimens were initially tested under load-control mode using load increments of 25 kN until the first flexural crack was observed on the beam surface. After cracking, the load increment was increased to 50 kN, depending on the expected capacity of the specimen. This loading procedure was continued until the total applied load reached approximately 75% of the predicted failure load obtained from the finite element analysis. Subsequently, the actuator was switched to displacement-control mode to

Provide better control of the post-cracking response and reduce the possibility of sudden brittle failure of the specimen.

2.5 Finite element deep beams modeling by using software program (ABAQUS):

The finite element analysis was conducted using ABAQUS/Standard, a general-purpose numerical analysis program capable of solving a wide range of linear and nonlinear structural problems. In this study, ABAQUS was employed to develop three-dimensional nonlinear models of reinforced concrete deep beams and to simulate their behavior under monotonic vertical loading up to failure.

2.5.1 Modeling steps

3D non-linear finite element model was created in ABAQUS by defining material Constitutive laws, element kinematics, boundary constraints, reinforcement interactions, and mesh density.

2.5.1.1 Concrete Constitutive Model

Non-linear concrete behavior was simulated using the Concrete Damaged Plasticity (CDP) framework, integrating isotropic damaged elasticity with compressive crushing and tensile cracking formulations. The calibrated CDP parameters are detailed in Table 3, with the modeled concrete volume shown in Figure 9.

Table 3: Concrete damage plasticity parameters for Abaqus material definition

Parameter	Value	Discerption
Ψ	35	Dilation angle
€	0.1	Eccentricity
fb_o/fc_o	1.16	The ratio of initial equiaxial compressive yield stress to initial uniaxial compressive yield stress
k	0.667	Ko the ratio of the second stress invariant on the tensile meridian
μ	0.007985	Viscosity parameter

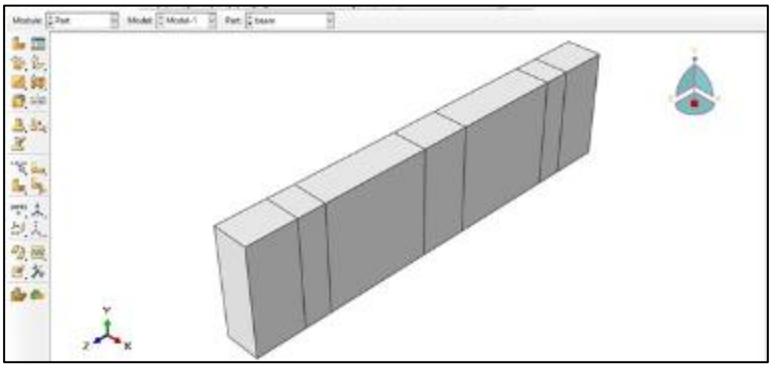

Figure 9: Concrete deep beam part

2.5.1.2 Reinforcement Steel Model

Reinforcing steel was modeled using an elastic–plastic constitutive law with strain hardening. True stress versus plastic strain curves were specified in ABAQUS to account for cross-sectional area reduction during post-yield loading.

2.5.1.3 Boundary Conditions

To prevent localized stress concentration at loading and support locations, steel bearing plates matching experimental dimensions were incorporated into the model. Loading was introduced via prescribed vertical displacement over the bearing plates, while support conditions were configured as pin and roller restraints to replicate testing conditions.

2.5.1.4 Element Formulations

A 3D modeling approach was adopted to improve structural accuracy over 2D plane-stress idealizations. The concrete domain and steel bearing plates were discretized using 3D 8-node linear brick elements with reduced integration (C3D8R) to avoid shear locking. Reinforcing bars were modeled using 2-node 3D linear truss elements (T3D2).

2.5.1.5 Bond Interaction

Steel reinforcement was fully embedded within the concrete matrix using the Embedded Region constraint in ABAQUS, assuming a perfect bond of interaction.

2.5.1.6 Meshing

A mesh sensitivity analysis determined an optimal element size of 50 mm (aspect ratio ￼,) balancing computational efficiency and numerical accuracy. The meshed FE models are shown in Figures 10 and 11.

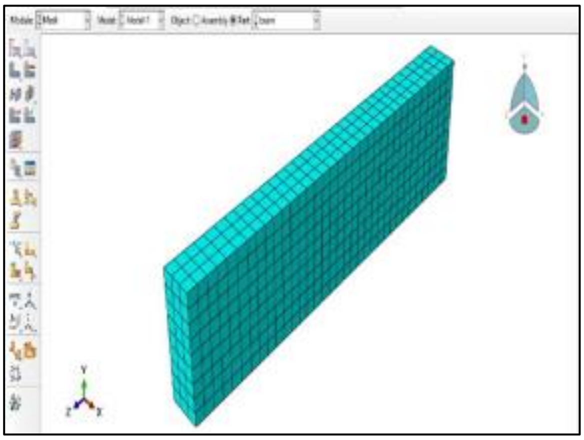

Figure 10: 1DB100bw meshed l

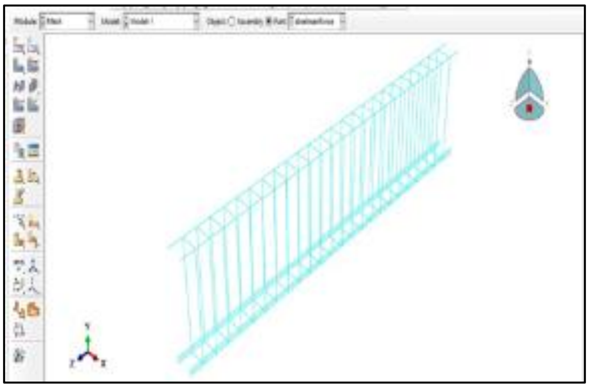

Figure 11: 1DB100bw meshed

2.5.2 Model Validation

The finite element model was validated against experimental data obtained from a previous study [11] involving nine reinforced concrete deep beam specimens. The comparison focused on load–deflection response, where close agreement confirmed the accuracy of the ABAQUS model in predicting global structural behavior.

2.6 Investigation of the Effects of Web Reinforcement and Beam Width on Plastic Strain:

2.6.1 Beam specimens considered in the investigation:

This section investigates the influence of web reinforcement and beam width on the development and distribution of plastic strain in reinforced concrete deep beams. The analysis focuses on comparing specimens with web reinforcement and constant width against specimens without web reinforcement but with proportionally increased beam width. The purpose of this comparison is to evaluate whether increased section width can improve crack resistance and reduce plastic strain concentration, even in the absence of conventional shear reinforcement.

The selected beams were examined using the developed ABAQUS finite element models. Attention was given to the onset of cracking, the magnitude of plastic strain, and the location of strain concentration zones near the load application and support regions. Figures (12) to (15) illustrate the geometry, reinforcement arrangement, and finite element representation of the beam specimens used in this part of the study.

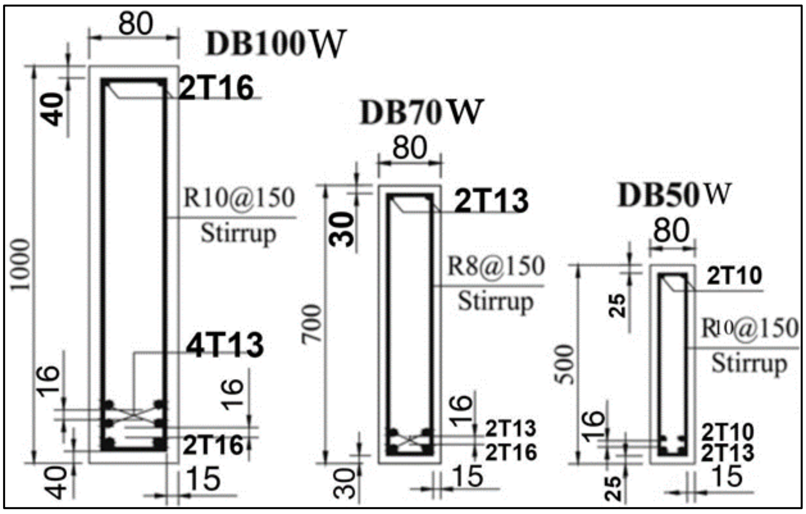

Figure 12: 2DBb beam-sections [11]

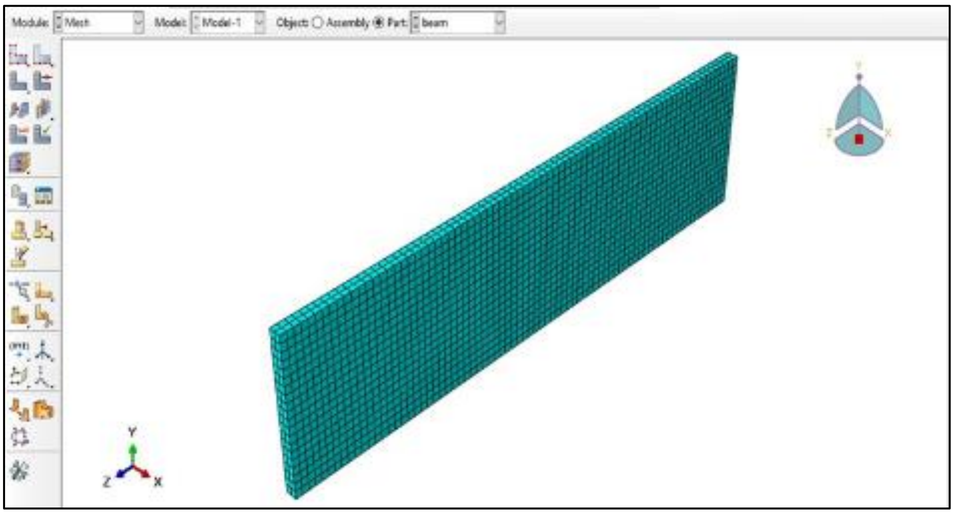

Figure 13: 2DB100w beam model

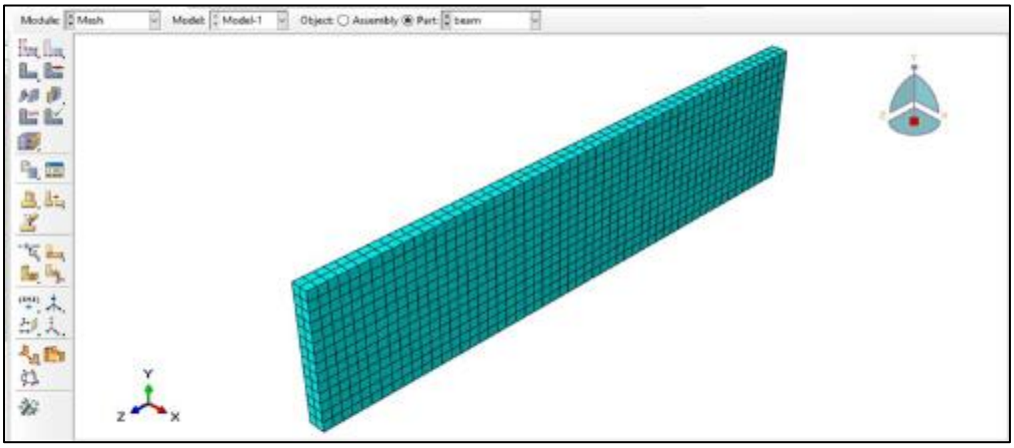

Figure 14: 2DB70w beam model

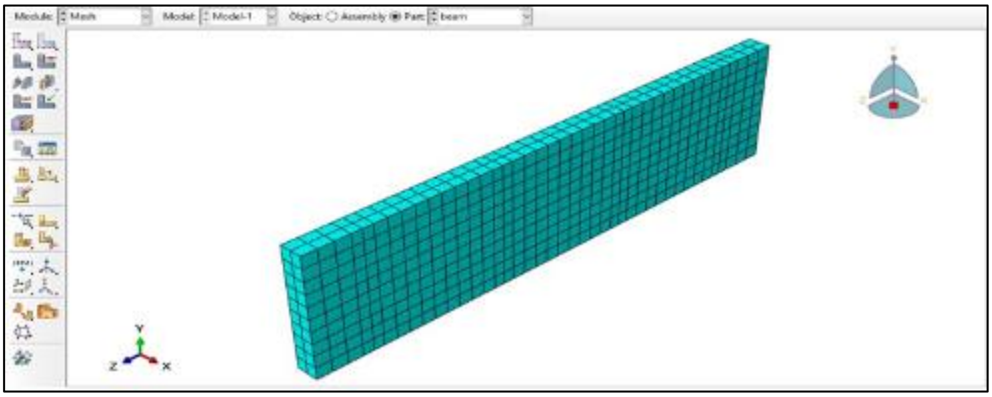

Figure 15: 2DB50w reinforcement model

2.6.2 Shear capacity of the section:

The shear capacity of the concrete section was evaluated in accordance with the provisions of ACI 318-05 [16]. The design check was performed to assess whether the concrete section and the provided reinforcement satisfied the required shear resistance. The nominal shear strength and minimum web reinforcement requirements were calculated using Equations (1) and (.2), respectively.

- $V_n < 10\sqrt{f_c'} \times (b_w d)$ (1)
- $Av > .0025 b_W s\ with\ s\,/5$ or 12 in (2)
- Where V_n : Nominal Shear Strength
- f'_c : Specified Compressive Strength of Concrete
- b_w **:** The width of the web (cross-sectional thickness) of the structural beam or wall
- d : Effective Depth
- Av *:* Cross-sectional area of shear/vertical reinforcement within a distance s
- s **:** The center-to-center spacing of the vertical reinforcement bars measured along the longitudinal axis of the member.

3 RESULTS AND DISCUSSION

This section presents the numerical results for the investigated reinforced concrete deep beams using ABAQUS. To establish model accuracy, the finite element predictions were validated against experimental load–deflection curves reported in the literature. Based on the validated model, a detailed parametric study was conducted to evaluate the effect of web reinforcement and beam width on the cracking behavior and plastic strain distribution across the beams.

3.1 Finite Element Analysis Results

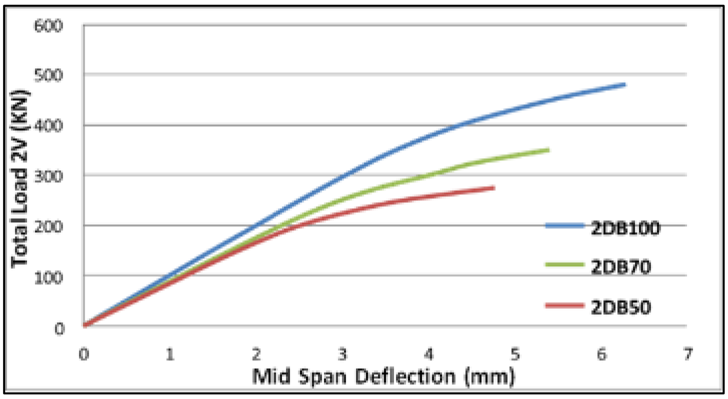

Figure 16: FEM result of deflection for group 1(with shear reinforcement and various width)

The finite element results for Group 1 are presented in Figure (16). The load–deflection curves show a consistent initial elastic stiffness for the specimens prior to reaching the elastic limit. Among the beams in this group, specimen 1DB50bw exhibited the largest midspan deflection, indicating lower stiffness compared with the deeper specimens. This behavior confirms the influence of beam depth on reducing deflection and increasing global stiffness.

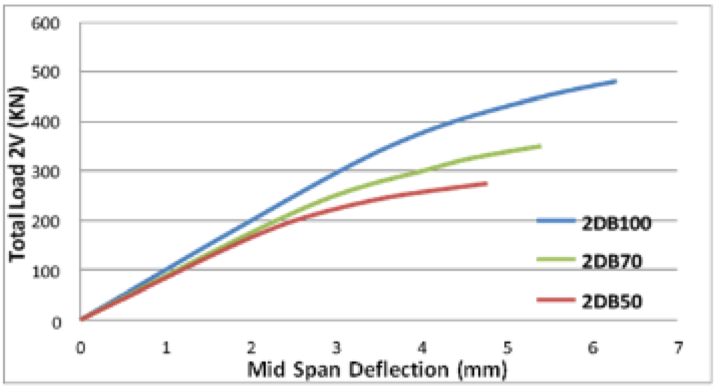

Figure 17: FEM result of deflection for group 2(without shear reinforcement and constant width

The finite element results for Group 2 are shown in Figure (17). Since the specimens in this group had constant width and no shear reinforcement, their numerical responses were generally similar. The results demonstrate that the absence of shear reinforcement, combined with constant beam width, produced comparable load–deflection behavior among the three specimens, with differences mainly associated with variations in beam depth.

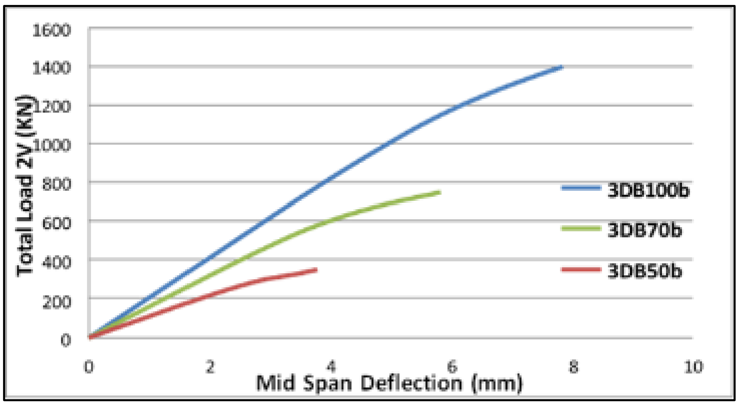

Figure 18: FEM results of group 3(without shear reinforcement and various width)

Figure (18) presents the finite element results for Group 3. The results indicate that the absence of top reinforcement reduced the ultimate load capacity when compared with beams provided with top reinforcement. In particular, the ultimate load decreased from approximately 1600 kN to 1400 kN. This reduction highlights the contribution of top reinforcement to improving flexural stiffness and enhancing the ultimate load resistance of reinforced concrete deep beams.

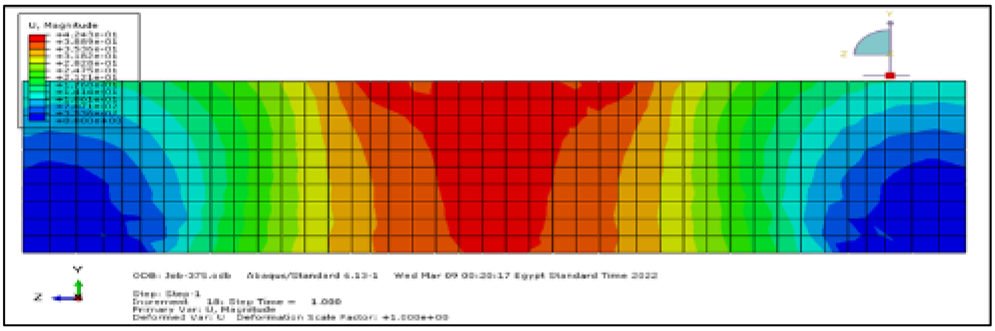

Figure 19: deformed shape of beam 1DB50bw under yield load

The deformed shape of a 1DB50bw specimen under the yield load is shown in Figure (19). The numerical displacement contour indicates that the maximum vertical deflection occurs near the midspan region, as represented by the red zone. The displacement gradually decreases toward the support regions, which is consistent with the expected flexural response of a simply supported beam subjected to two-point loading.

3.2 Comparison Between Numerical Predictions and Experimental Literature Data

The finite element model was validated by comparing numerical load–deflection predictions with experimental results reported by Ning Zhang et al. (2007) [11] for nine reinforced concrete deep beams. Comparisons for Groups 1, 2, and 3 are illustrated in Figures 20, 21, and 22, respectively. Evaluation was conducted at the load corresponding to maximum pre-yield deflection, confirming the model's accuracy in capturing pre-yield structural behavior

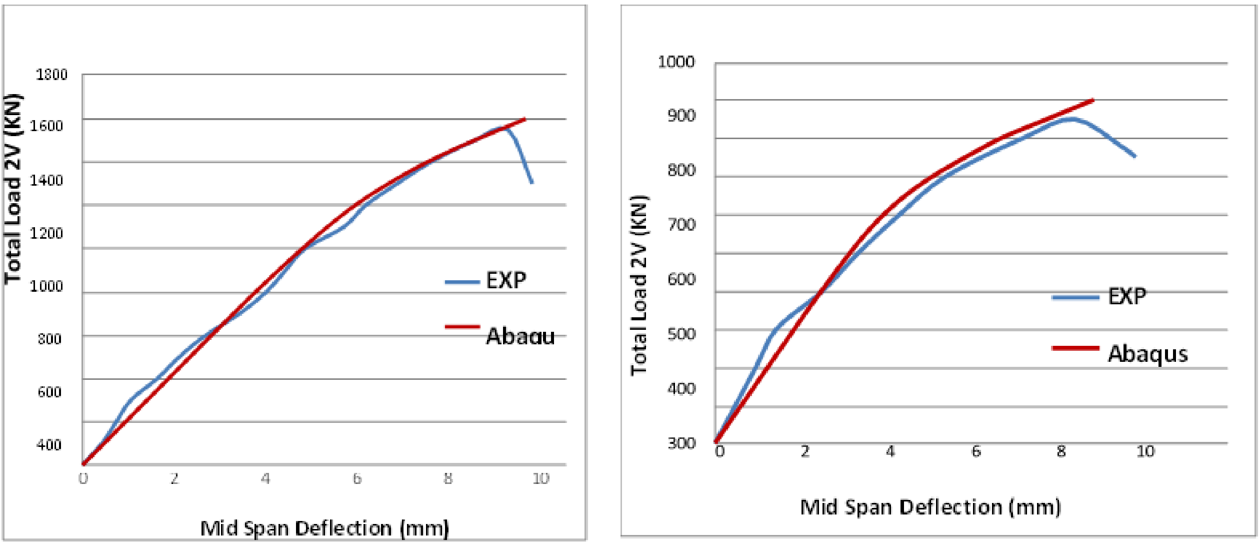

a b

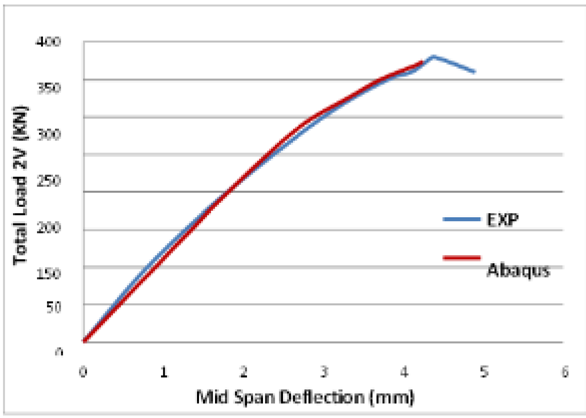

c

Figure 20: Experimental and FEM deflection results of group 1 1DB100bw, (b) 1DB70bw, (c) 1DB50bw

Figure 20 demonstrates close agreement between experimental and numerical load–deflection curves for Group 1. Specimen 1DB100bw exhibited a pre-yield peak load of 1500 kN experimentally and 1600 kN numerically (0.1% error), confirming the model's predictive accuracy for shear-reinforced deep beams with varying web widths.

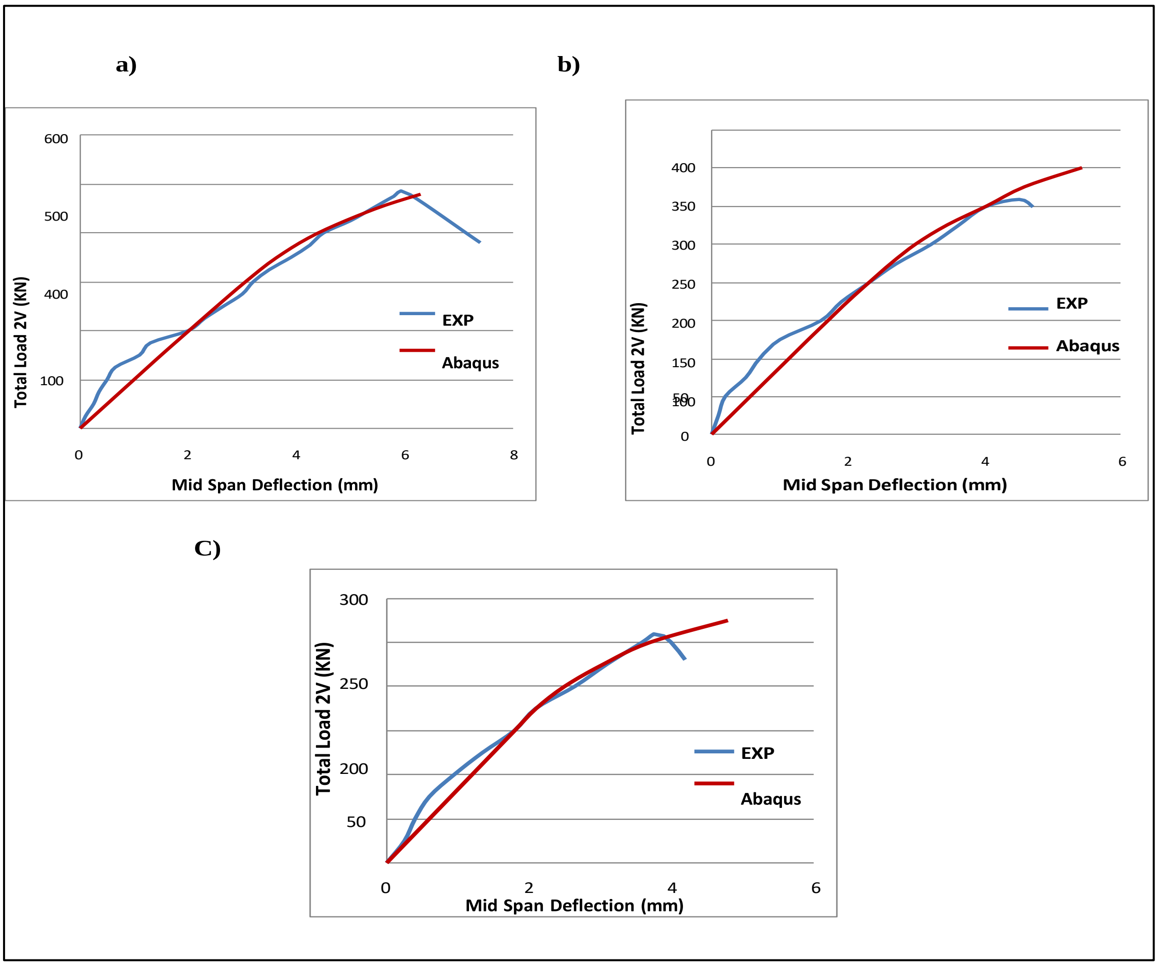

Figure 21: Experimental and FEM deflection results of group 2 (a) 2DB100, (b) 2DB70, (c) 2DB50

Figure 21 shows an acceptable agreement between experimental and FEM load–deflection responses for Group 2. For the representative specimen, the pre-yield load was 500 kN experimentally versus 485 kN numerically (~0.15% difference), confirming model reliability for beams without shear reinforcement and with constant width

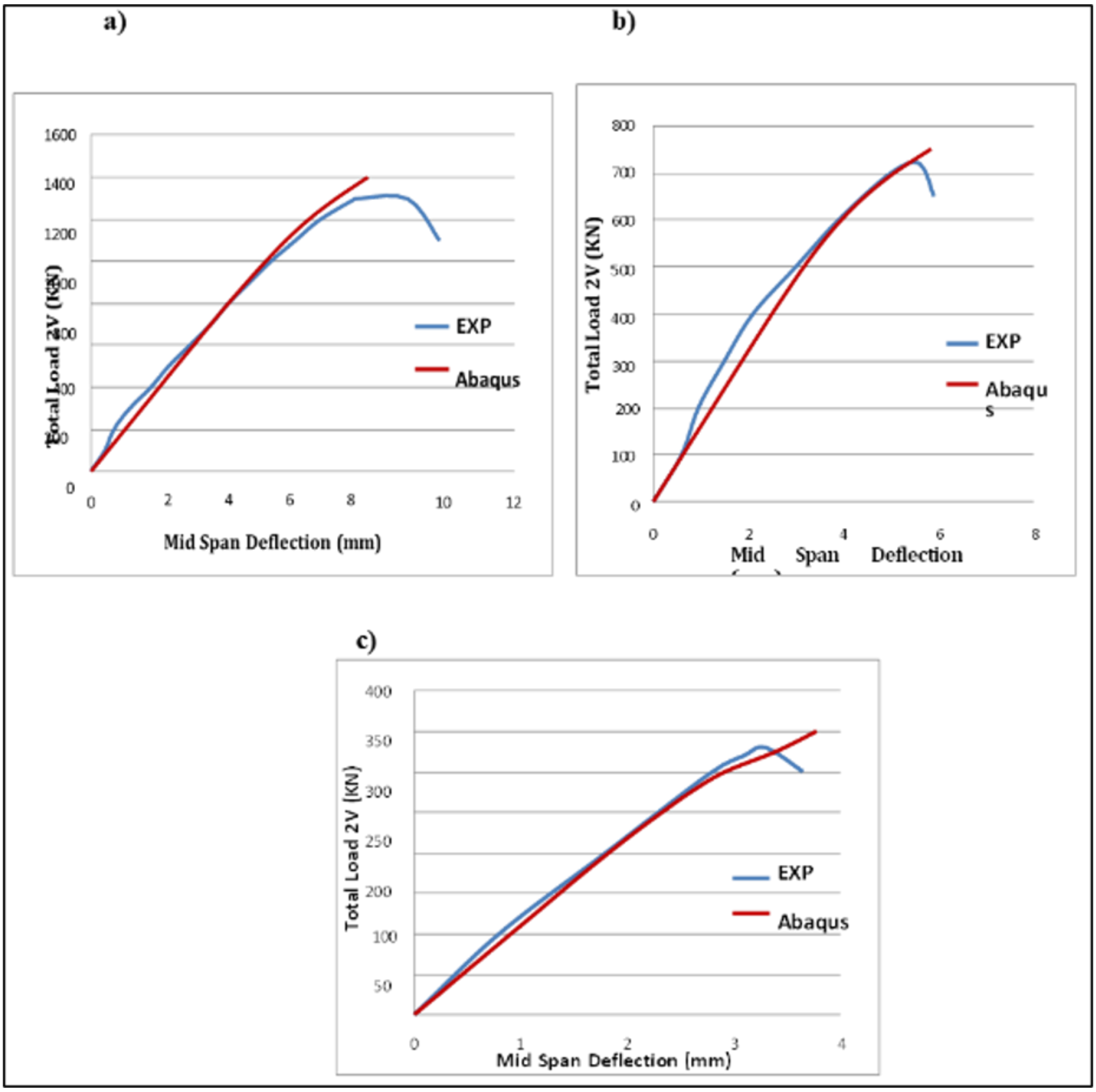

Figure 22: Group 3 (a) 3DB100b, (b) 3DB70b, (c) 3DB50b

Figure 22 demonstrates a good agreement between experimental and numerical load–deflection responses for Group 3. The pre-yield load reached 1350 kN experimentally compared to 1400 kN numerically (~0.5% difference), reinforcing the model's capacity to predict the behavior of beams without shear reinforcement and with scaled web widths.

3.3 Results and Discussion of Web Reinforcement and Beam Width Effects on Crack Development:

3.3.1 Determination of the Optimum *h/b* Ratio for the Study:

The height-to-width ratio, *h/b*, was examined to evaluate the influence of beam width on shear capacity and crack development. For beams without web reinforcement, the selected *h/b* ratios were 4.4, 3.1, and 2.2, whereas the corresponding ratios for beams with web reinforcement were 12.5, 8.8, and 6.3, respectively. These ratios were compared to determine the most critical section configuration for evaluating the combined effects of beam width and web reinforcement.

Table 4: Section shear capacity of different rate of h/b for beams without web reinforcement for beam 1:

h/b	Depth (mm)	Required width (mm)	Section shear resistance rate (KN/mm)
4.4	1000	230	9.298
	700	160	6.57
	500	115	4.67
3.1	1000	325	13.14
	700	225	9.23
	500	160	6.5
2.2	1000	455	18.39
	700	320	13.125
	500	230	9.34

As presented in **Table 4**, the h/b ratio of 4.4 was selected as the most critical case when compared with ratios of 3.1 and 2.2. This ratio produced the lowest section of shear resistance relative to beam depth and was therefore considered appropriate for assessing the critical response of beams without web reinforcement.

3.3.2 Determination of required web reinforcement for beams with constant width:

The required web reinforcement for beams with constant width was determined from the shear capacity calculations. The results indicate that the beams were reinforced using at least the minimum reinforcement percentage required by the design provisions, as summarized in **Table 4**.

Table 5: Check of shear capacity of concrete section for beams with shear reinforcement:

Beam designation	Applied shear force (kN)	Section shear capacity (kN)	Minimum required shear reinforcement area(mm^2)	Provided shear reinforcement area(mm^2)
2DB100w	2400	3313	30	156
2DB70w	1266.67	2325.5	30	101
2DB50w	1066.67	1642.17	30	156

The results in Table 5 show that the provided shear reinforcement area exceeded the calculated minimum requirement for the investigated beams. Consequently, the use of web reinforcement enhanced the shear resistance of the sections and contributed to the overall load-carrying capacity of the beams.

Table 6: comparison between 2DBw group and 3DBb group:

Beam designation	Stirrups	Dimension H*B(mm)	Failure load (2VkN)	Initial flexural cracking load(2VkN)	Ultimate stress (N/mm^2)	Failure mode	Plastic strain
2DB100w	With stirrups	1000X80	1800	200	52	SC	0.01347
2DB70w		700X80	950	150	52	SC	0.007646
2DB50w		500X80	800	150	52	SC	0.01435
3DB100b		1000X230	3600	300	55.5	SC	0.004736

3DB70b	Without stirrups	700X160	2000	400	52	SC	0.00486
3DB50b		500X115	1000	200	52	SC	0.01017

The comparison between the 2DBw and 3DBb groups indicates that beams with web reinforcement and a constant width of 80 mm exhibited lower initial cracking loads than beams without stirrups but with increased section width. This behavior suggests that the relatively small beam width made the reinforced specimens more susceptible to early crack formation, despite the presence of shear reinforcement.

In addition, the beams with web reinforcement and smaller width developed higher plastic strain levels, as illustrated in Figures (26), (28), and (30). The wider distribution of plastic strain reflects greater crack development and a comparatively lower flexural resistance.

Conversely, beams without web reinforcement but with larger widths showed higher initial cracking loads, greater failure loads, and lower plastic strain values. The plastic strain distributions shown in Figures (30), (32), and (34) demonstrate that increasing beam width improved crack resistance and enhanced the overall flexural capacity of the deep beams

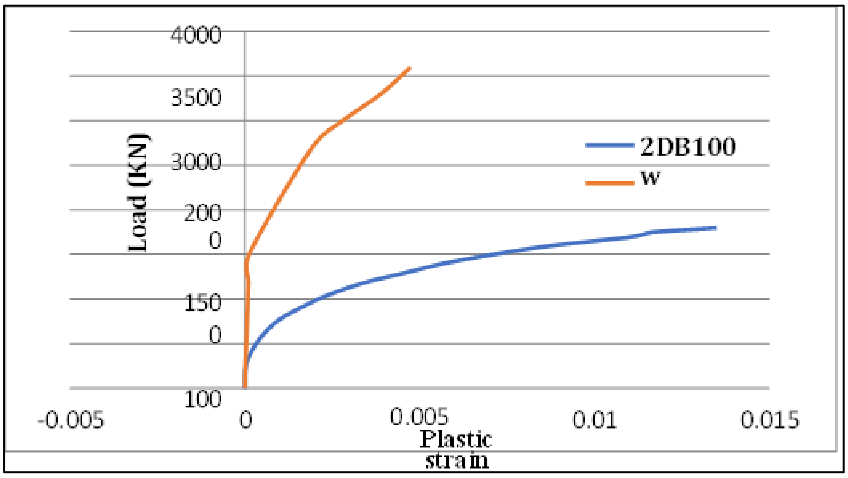

Figure 23: Plastic strain comparison between 2DB100w and 3DB100b

Figure (23) compares the plastic strain development of specimens 2DB100w and 3DB100b. Specimen 2DB100w, which included web reinforcement and had a constant width, exhibited plastic strain initiation at a lower load level of approximately 200 kN. In contrast, specimen 3DB100b, which had no web reinforcement but a larger width, developed initial cracking at approximately 300 kN. This indicates that the increased beam width improved resistance to early crack formation.

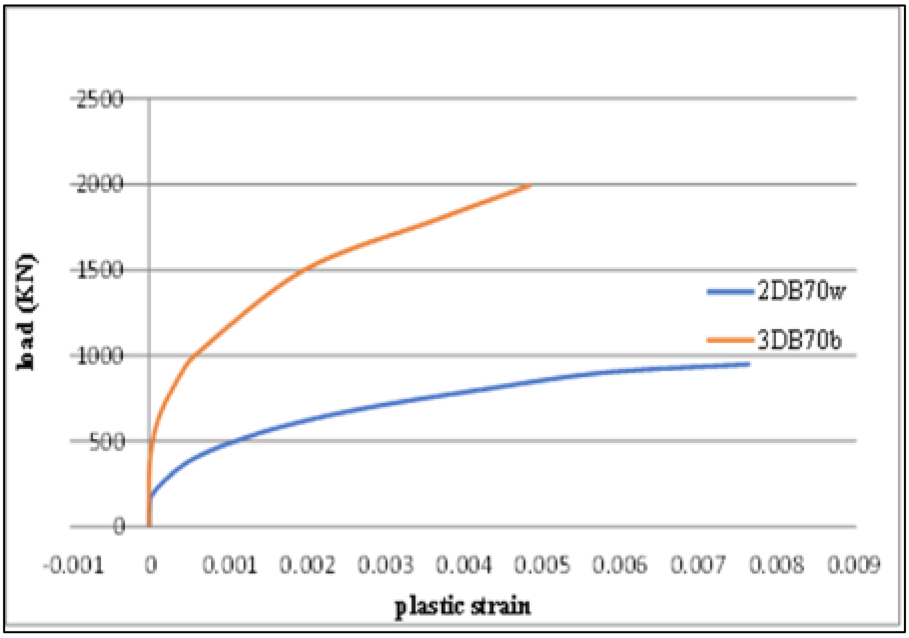

Figure 24: Plastic strain comparison between 2DB70w and 3DB70b

A similar trend is observed in Figure (24) for specimens 2DB70w and 3DB70b. Specimen 2DB70w showed earlier plastic strain development at approximately 150 kN, whereas specimen 3DB70b exhibited a higher initial cracking load of approximately 400 kN. This comparison further confirms that a larger beam width can delay crack initiation and reduce plastic strain concentration.

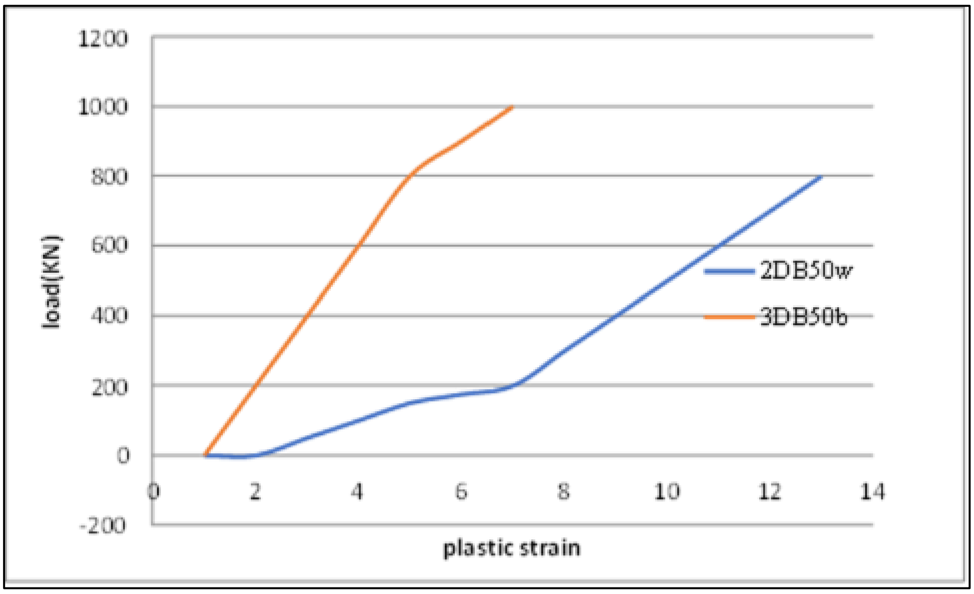

Figure 25: Plastic strain comparison between 2DB50w and 3DB50b

Figure (25) compares specimens 2DB50w and 3DB50b. Specimen 2DB50w, with web reinforcement and constant width, developed plastic strain at a lower load level of approximately 150 kN. Conversely, specimen 3DB50b, without web reinforcement but with increased width, exhibited an initial cracking load of approximately 200 kN. The results indicate that increased width contributed to improved crack resistance even in the absence of stirrups.

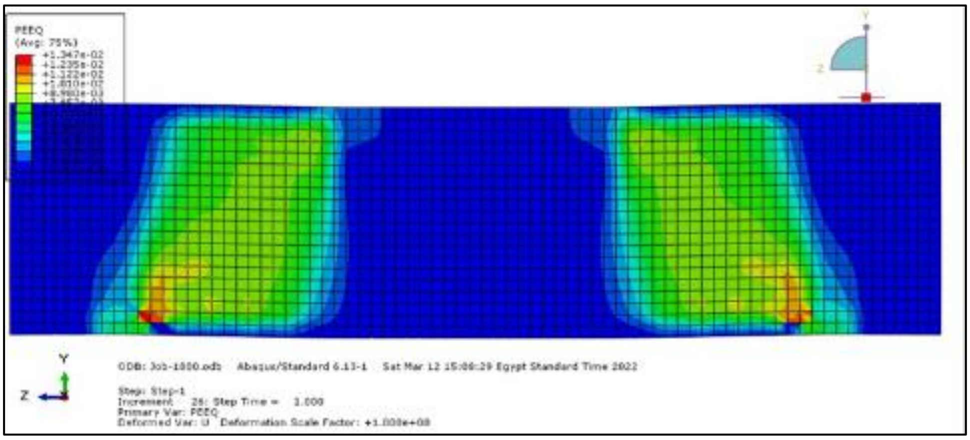

Figure 26: Plastic strain in 2DB100w

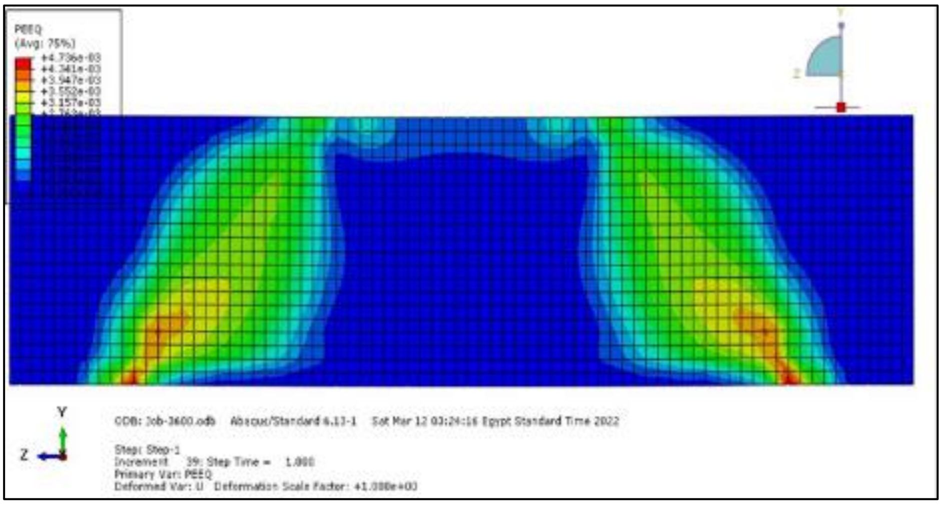

Figure 27: Plastic strain in 3DB100

Figures (26) and (27) illustrate the plastic strain distributions for specimens 2DB100w and 3DB100b, respectively. The results show that plastic strain developed primarily along the diagonal compression path extending from the loading points toward the support regions, which is consistent with the expected strut action in reinforced deep beams.

The comparison indicates that the specimen with web reinforcement and smaller width exhibited a wider plastic strain region than the wider specimen without stirrups. This suggests that increased beam width contributed to reducing strain concentration and improving crack resistance.

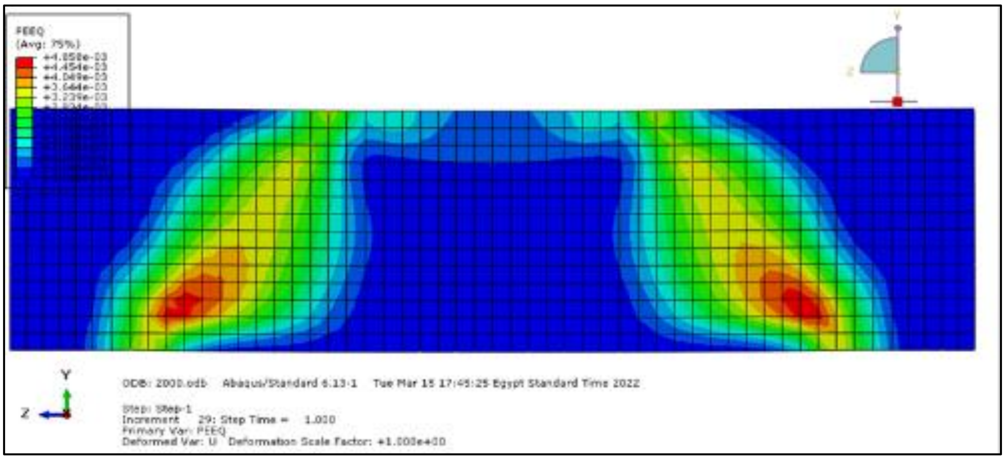

Figure 28: Plastic strain in 2DB70

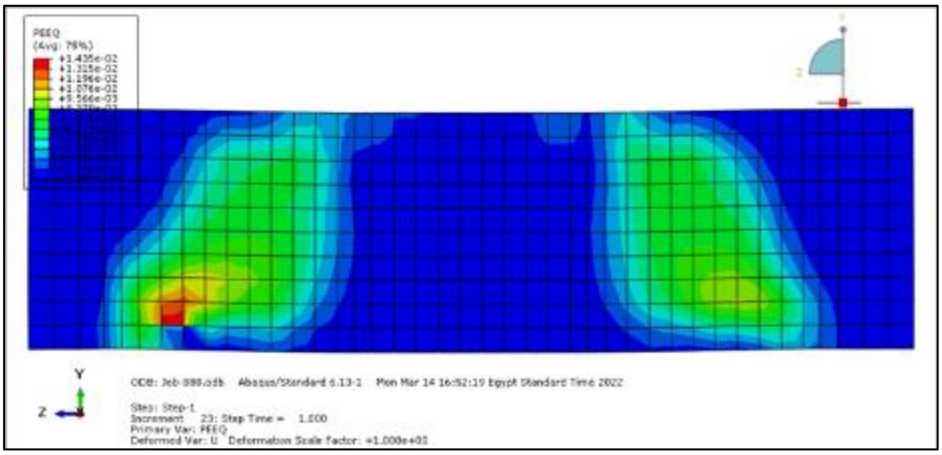

Figure 29: Plastic strain in 3DB70b

Figures (28) and (29) present the plastic strain distributions for specimens 2DB70w and 3DB70b, respectively. Like the 1000 mm beam specimens, the plastic strain developed mainly along the diagonal load-transfer path between the applied loads and the supports. The concentration of strain in

these regions confirm the dominant role of diagonal compression in the shear behavior of deep beams.

The beam provided with web reinforcement showed a broader distribution of plastic strain, whereas the wider beam without stirrups exhibited reduced strain concentration. This behavior indicates that increasing beam width can enhance the effective compression zone and delay the progression of cracking.

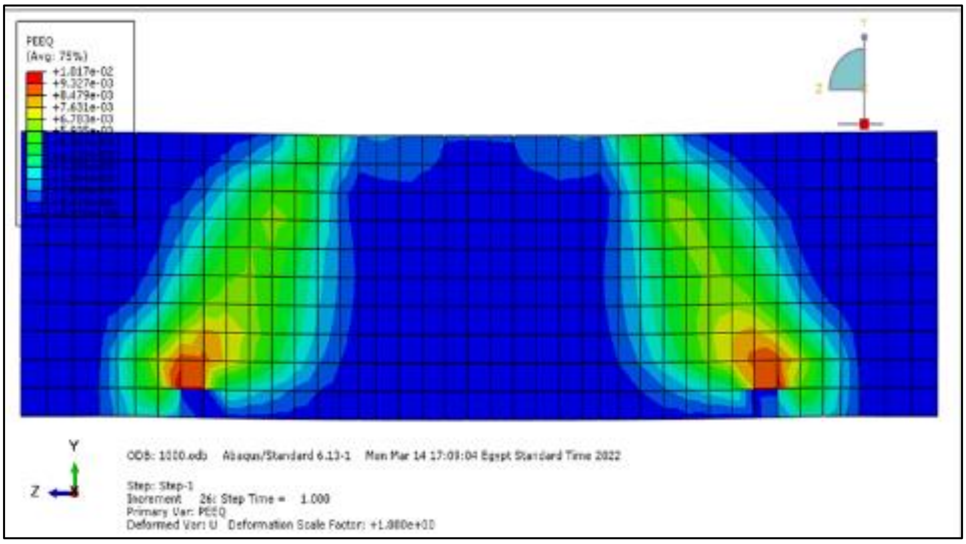

Figure 30: Plastic strain in 2DB50w

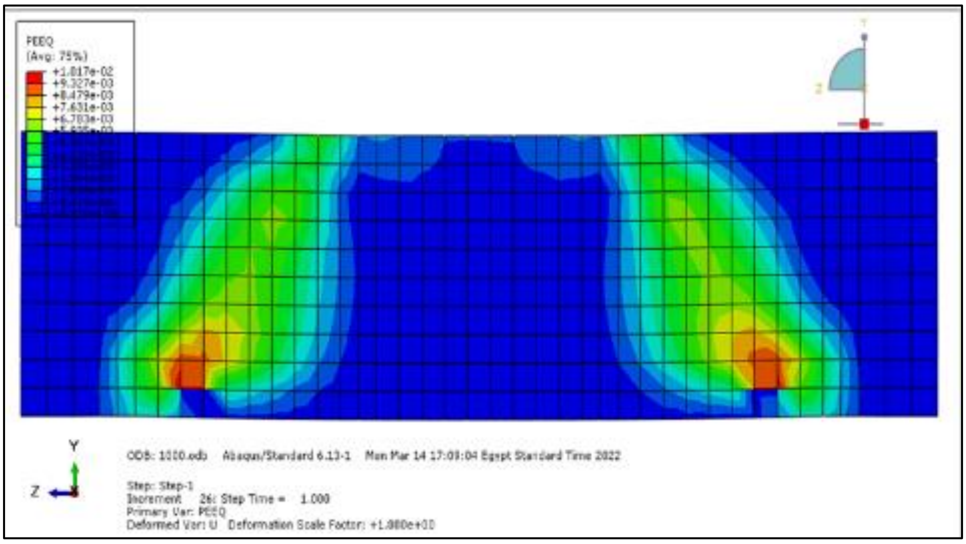

Figure 31: Plastic strain in 3DB50b

Figures (30) and (31) show the plastic strain distributions for specimens 2DB50w and 3DB50b, respectively. The numerical results indicate that strain localization occurred near the load application and support regions, following the expected diagonal strut mechanism. This response is consistent with the behavior observed in larger beam specimens.

Overall, the plastic strain contours demonstrate that beams with increased width developed lower and more localized plastic strain than the narrower beams with web reinforcement. This confirms that beam width has a significant influence on crack control, strain distribution, and the load-transfer mechanism of reinforced concrete deep beams.

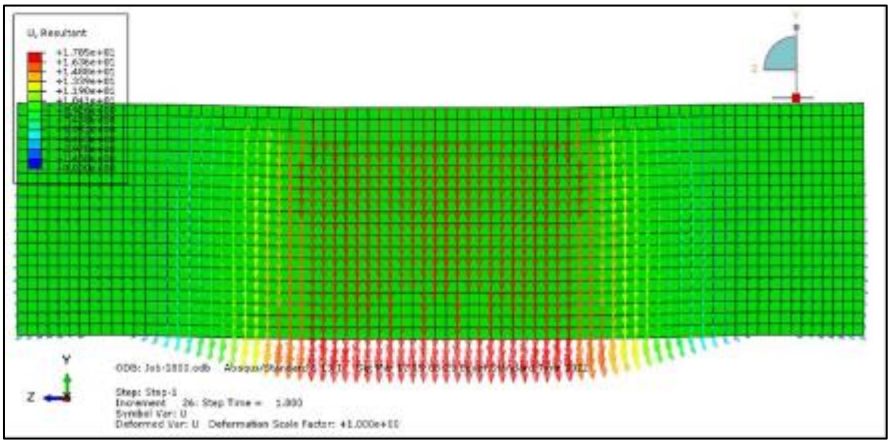

Figure 32: Compressive force path for 2DB100w

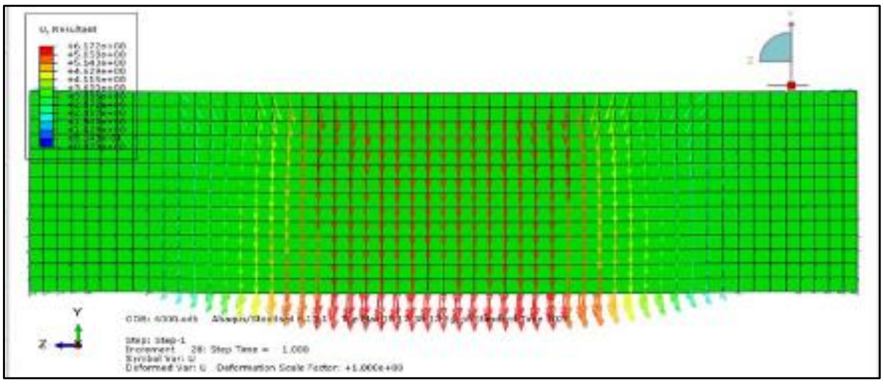

Figure 33: Compressive force path for 2DB70w

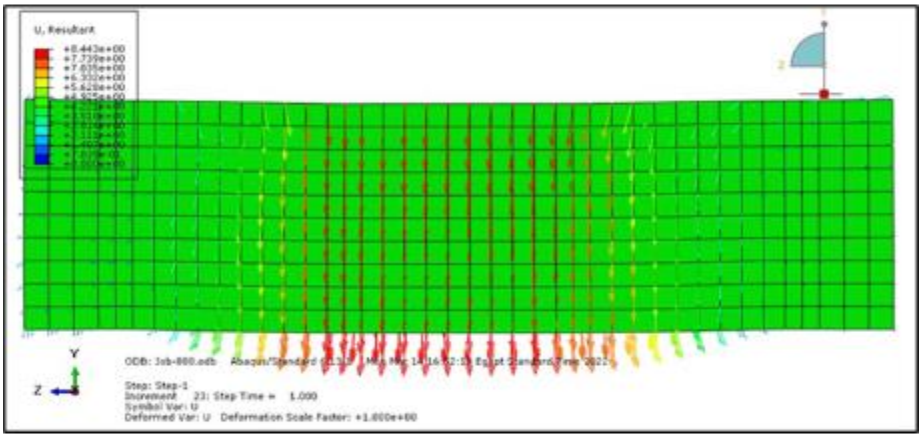

Figure 34: Compressive force path for 2DB50w

Figures (32), (33), and (34) illustrate the compressive force paths developed within specimens 2DB100w, 2DB70w, and 2DB50w, respectively. The results show that the internal load-transfer mechanism is governed by diagonal compression struts extending from the applied loading regions toward the supports. These compressive stress trajectories define the primary force flow within the deep beams and confirm the dominant contribution of strut action in resisting the applied loads.

4 CONCLUSION

This study examined the structural behavior of reinforced concrete deep beams through three-dimensional nonlinear finite element analysis using ABAQUS. The investigation focused on the effects of beam size, web reinforcement, and beam width on load–deflection response, crack initiation, plastic strain distribution, and internal force-transfer mechanisms. The Concrete Damaged Plasticity model was employed to represent the nonlinear response of concrete, and the numerical models were validated using available experimental results.

The comparison between the experimental observations and finite element predictions showed a high level of agreement in the load–deflection response. This confirms that the developed ABAQUS model can predict the global behavior of reinforced concrete deep beams with satisfactory accuracy. The results further indicated that increases in beam depth and width enhance stiffness, improve load-carrying capacity, reduce midspan deflection, and delay the onset of cracking. Specimens with proportionally increased width and without stirrups demonstrated lower plastic strain values and greater crack resistance than narrower specimens provided with web reinforcement.

The plastic strain contours and compressive force-path results confirmed that the behavior of deep beams is governed primarily by diagonal compression strut action between the loading points and supports. These findings highlight the significant role of beam geometry, particularly width, in controlling crack development, reducing strain concentration, and improving the overall structural performance of reinforced concrete deep beams.

STATEMENTS ON COMPLIANCE WITH ETHICAL STANDARDS

Acknowledgments

The authors would like to acknowledge the Department of Structure at Sudan University of Science and Technology for supporting the numerical simulation work. Special thanks are also extended to colleagues and reviewers for their valuable feedback and insightful suggestions during the preparation of this manuscript.

Funding Source

No funding source for this study.

Disclosure of conflict of interest

The authors declare that no conflict of interest exists regarding the publication of this manuscript

REFERENCES

[1] Standard textbook/general background reference on reinforced concrete behavior and mechanics.

[2] Standard background reference on deep beam span-to-depth ratios and non-linear stress distribution.

[3] Abtan, Y. O., & Hassan, A. A. *Behavior and theoretical review of reinforced concrete deep beams*. (Cited for conventional beam theory limits, Table 1, and Strut-and-Tie Method steps).

[4] Standard background reference on compressive strut action and shear deformation mechanisms.

[5] BS 8110: *Structural use of concrete*. British Standards Institution.

[6] Comité Euro-International du Béton (CEB-FIP). *Model Code for Concrete Structures*.

[7] ACI Committee 318. *Building Code Requirements for Structural Concrete (ACI 318) and Commentary (Appendix A)*. American Concrete Institute.

[8] Standard background reference on strut-and-tie idealization and nodal zone definitions (Figure 1).

[9] Standard background reference on member size and geometric scale influences (Figure 2).

[10] Ismail, M. *Experimental and numerical investigation into shear behavior and compressive force paths of reinforced concrete deep beams*. (Cited for Compressive Force Path concept, Figures 3).

[11] Zhang, N., et al. (2007). *Experimental study on load-deflection and structural performance of reinforced concrete deep beams*

[12] Qingfu, L., Wei, Z., & Yihang, C. Parameter calculation and verification for the ABAQUS concrete damaged plasticity model.

[13] Cuong-Le, T., Le-Minh, H., & Sang-To, T. Nonlinear concrete damaged plasticity model calibration for structural engineering applications.

[14] Öztemel, A., & Sümer, Y. Numerical investigation of reinforced concrete deep beams reinforced with fiber-reinforced polymer (FRP) bars.

[15] Elkholy, S., Salem, H., & Godat, A. Finite element modeling of deep beams incorporating recycled coarse aggregate concrete and steel fibers.

[16] ACI Committee 318. Building Code Requirements for Structural Concrete (ACI 318-05) and Commentary. American Concrete Institute, 2005.

[17] Rai, A. Nonlinear finite element modeling of reinforced concrete deep beams using the Concrete Damaged Plasticity model in ABAQUS. (Cited for CDP implementation, test setups, Figures 5–7, 12).